# RAIL FATIGUE AND THE ROLE OF IMPACT FORCES

**Martin Murray**

**BE, PhD, CPEng, MIEAust, RPEQ**

**Queensland University of Technology, Australia**

**KCPM Consulting Pty Ltd, Brisbane, Australia**

## SUMMARY

Fatigue of the steel in rails continues to be of major concern to heavy haul track owners despite careful selection and maintenance of rails. The persistence of fatigue is due in part to the erroneous assumption that the maximum loads on, and stresses in, the rails are predictable. Recent analysis of extensive wheel impact detector data from a number of heavy haul tracks has shown that the most damaging forces are in fact randomly distributed with time and location and can be much greater than generally expected. Large-scale Monte-Carlo simulations have been used to identify rail stresses caused by actual, measured distributions of wheel-rail forces on heavy haul tracks. The simulations show that fatigue failure of the rail foot can occur in situations which would be overlooked by traditional analyses. The most serious of these situations are those where track is accessed by multiple operators and in situations where there is a mix of heavy haul, general freight and/or passenger traffic. The least serious are those where the track is carrying single-operator-owned heavy haul unit trains. The paper shows how using the nominal maximum axle load of passing traffic, which is the key issue in traditional analyses, is insufficient and must be augmented with consideration of important operational factors. Ignoring such factors can be costly.

## 1 INTRODUCTION

Mitigation of the effects of tension stresses in rails to avoid fatigue cracking is a major concern for rail designers and maintainers. Careful analysis of the wheel-rail forces that cause those tension stresses is essential at the design stage to minimise the likelihood of fatigue occurring and to reduce rail maintenance costs.

The foot of the rail sustains the largest stresses due to flexing of the rail as each wheel passes. Those stresses cycle rapidly from zero to a small compression stress then to a high peak of tension and back again, many millions of times during the life of a rail in heavy haul track. These are ideal conditions for so-called mechanical fatigue failure of the steel in the rails, caused by the propagation of cracks from small defects in the steel. Catastrophic propagation of such cracks leads to rail breaks and possible derailment of trains, which can be tragic and expensive.

It is essential, therefore, for track designers and rail selectors to be able to reliably determine the tension stresses in the rail and ensure that those stresses do not exceed safe fatigue limits. If occasional large wheel-rail forces do cause the limit to be exceeded, then the designer must ensure that the damage caused by those stresses does not accumulate to the point where a crack may propagate through the rail with disastrous consequences.

Clearly it is critical for designers to know the distribution of wheel-rail forces and rail stresses with a high degree of confidence, and to know the many factors which can have a significant effect on those forces and stresses.

## 2 NOTATION

BOEF: beam on elastic foundation analysis.

CWR: continuously welded rail.

E: elastic (Young's) modulus of steel.

I: moment of inertia of rail section.

k: track modulus.

M: bending moment in rail.

MGT: million gross tonnes.

$N_i$: number of cycles of stress in rail.

P: wheel-rail contact force.

$S_i$: magnitude of stress in each cycle.

SFT: stress free temperature of rail.

TAL: tonnes axle load.

UTS: ultimate tensile strength of steel in rail.

$W_{failure}$: accumulated fatigue damage at failure.

WID: wheel impact detector, for wheel impacts.

x: distance along rail from wheel-rail contact.

β: a measure of the stiffness of rail & track.

## 3 RAIL STRESSES

### 3.1. Usual Method of Fatigue Checking

Rails in heavy haul track fall into the category of "high cycle fatigue", which covers between $10^6$ and $10^8$ cycles of loading during the life of the rail [1]. There is a general belief that beyond about $10^7$ cycles steel develops an endurance limit, and if stresses do not exceed that limit the steel will never fail due to cyclic loading alone [2]. In the selection of rails for track this limit is often expressed as a percentage of the uniaxial tension strength (UTS) [3, 4]. For stresses below the endurance limit, plastic action may occur but strain hardening raises the yield stress so that plastic action ceases and the steel carries additional load cycles without further damage; this process is known as "shakedown" and is an important characteristic in rails. Similarly, if cracks are present in the steel but stresses are below the endurance limit, then plastic action at the tip of the crack can blunt the crack tip, and propagation of the crack ceases.

The rail foot experiences the highest tension bending stresses, so if the peak stresses in the foot exceed the endurance limit then shakedown will not occur and fatigue damage will accumulate with every stress cycle. Crack initiation, propagation and a broken rail become highly likely, the consequences of which can be disastrous.

To avoid this condition, rail designers follow a well-established process. First, the design dynamic load is determined by multiplying the wheel-rail static force (exerted by the weight of the train through the wheel-rail interface) by a dynamic load factor. That factor accounts for: the bouncing of the train due to roughness of the track and/or wind and other dynamic actions within the train consist; the speed of the train; the type of train vehicle; and the importance of the train-track system.

Using a conventional beam-on-elastic-foundation (BOEF) analysis, the bending stress in the rail is then calculated from the design dynamic load. Those stresses are affected by track stiffness, sleeper spacing, and rail properties. In these calculations, allowance is made for variations laterally and longitudinally in the support provided by the track substructure. The designer then adds in additional tension caused by torsion and lateral bending effects in the rail, as well as temperature induced tension in continuously welded rail (CWR). Finally an allowance is made for likely tension stresses retained in the cross section from the manufacturing process, known as residual stresses.

The sum of all these tension stresses is then compared to the chosen fatigue/endurance limit. If the stresses are less than the limit, then the rail is deemed to be unlikely to develop bending fatigue cracks in the rail foot and all is assumed to be well.

### 3.2. Problems with Materials

Despite the care taken in attempting to determine, and to limit, all the stresses in the rail, fatigue cracking in the rail foot persists in appearing, even in well-designed rails. One of the factors causing this uncertainty is the fatigue resistance of the steel in the rails.

As described above, rail steel is generally assumed to have a given, determinable endurance limit beyond about $10^7$ cycles of loading. Much of the early testing which appeared to establish this limit was based upon fatigue tests which did not progress much beyond $10^7$ or $10^8$ cycles, because mechanical fatigue testing is expensive and time consuming.

However, the newer method of ultrasonic fatigue testing is relatively cheap and quick and tests of rail steels to $10^{10}$ cycles have been undertaken [1]; Figure 1 shows rail steel's fatigue behaviour when it is pushed beyond that boundary of $10^7$ cycles. The test results showed no fixed endurance limit; instead the stress at fatigue failure for a given number of load cycles continued to decrease linearly with the log of the number of cycles.

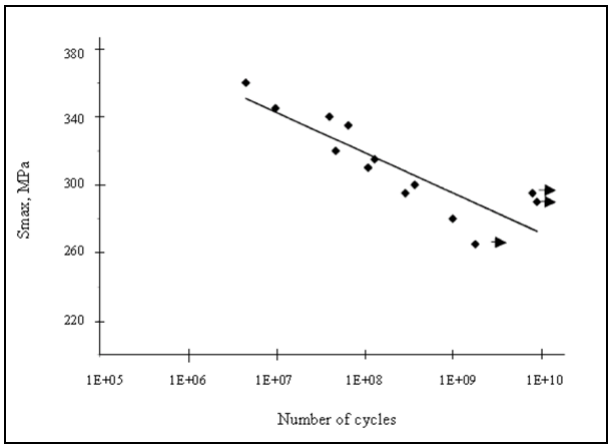


**Figure 1 : Fatigue of 700 Grade Rail Steel [1]**

The difference in fatigue strength between $10^6$ and $10^9$ load cycles in Figure 1 is approximately 70 MPa, which can be significant in heavy haul track. To illustrate: on a busy suburban commuter line carrying say 100 trains per track per day, the rail receives 0.6 million cycles of load per year; but heavy haul lines in Australia usually carry well over 100 million gross tonnes per annum (MGT/a) of traffic, which can result in over 5 million load cycles per annum in the rail. As a result, $10^8$ cycles of loading in the life of a rail is not out of the question for well-maintained heavy haul rails in which a life span of up to 1,500 MGT of total traffic is becoming achievable. That limit that may go even higher with better grinding regimes, continual fine tuning of wheel-rail profiles, and the like.

The operation of heavy haul lines is pushing rails further and further to the right in Figure 1 where fixed endurance limits do not really apply.

### 3.3. Problems with Loads

The established process by which fatigue in rails is hopefully avoided, as described in section 3.1, assumes that the maximum loads which the rail experiences under passing trains can be predicted with some certainty. This assumption is based on wheel-rail force data from certain field tests on tracks around the world.

However, such testing is very expensive and there is a huge range of traffic types on the world's many different types of tracks, so the number of field tests relevant specifically to heavy haul is not large. The assumption that maximum wheel-rail forces are predictable is therefore not based on statistically defensible data. But recently a huge source of reliable, repeatable data has become available.

Over the last 15 years or so, the use of wheel impact detectors (WID) on heavy haul lines has become common. WIDs have been installed to detect wheel-rail impact forces with the intention that serious tread defects in wheel sets can be identified, removed from service, and rectified. In the process WIDs produce enormous quantities of data because they monitor the force from every wheel on every train which passes the WID site.

There is therefore a rich mine of information in that data about the range, magnitude and rate of occurrence of every single one of the static and dynamic forces which a heavy haul track experiences.

Since 2005, annualised sets of data have been made available to the author from WID installations on a number of heavy haul lines around Australia [5]. This WID data contains both the static wheel-rail force (due to gravity forces on the vehicle) and the maximum wheel-rail force, from every wheel. Subtracting the static force from the maximum force gives the "incremental impact force", which is the component of the wheel-rail force that is due to dynamic action of the vehicle and wheel defects. Figure 2 shows the resulting distributions of incremental impact forces for five sites, nominated as A1, A2, B, C1 and C2, located in three different Australian states.

The five sites are all heavy haul, have similar track structures, track maintenance standards, train speeds and traffic volumes, and carry either iron ore or coal. The most obvious differences between them relate to axle load, ranging from 25 TAL at site C1 to 35 TAL at site B, but there are also significant differences related to operational practices [5].

In Figure 2, incremental forces above about 100kN can be shown to be due primarily to wheel defects such as wheel tread flats or out-of-round wheels.

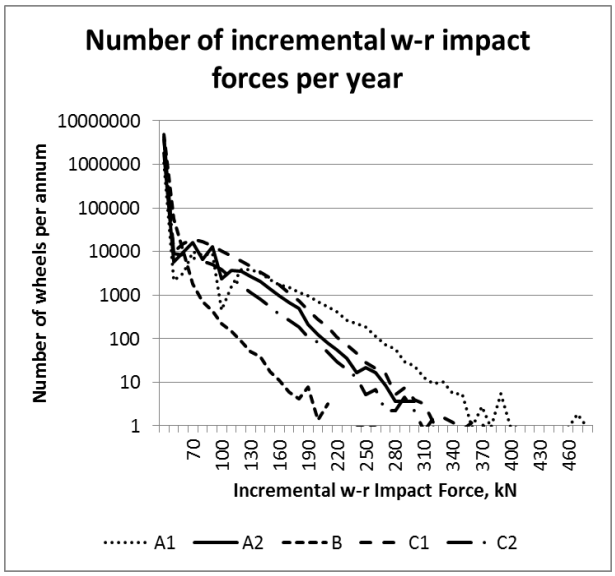


**Figure 2 : Impact Wheel-rail Forces on Heavy Haul Lines [5]**

The data in Figure 2 has been analysed extensively elsewhere [5] but there are four points of interest in the graph which are relevant with respect to rail stresses and fatigue:

a. In Figure 2, the maximum force measured over one-year for each of the five sites varies widely, from a low of 210kN at site B to a high of 390kN at site A1. Table 1 lists these forces in order of the nominal static axle load at each of the five sites. Normally it is expected that higher impact forces would be associated with higher static axle loads, but Table 1 shows a reverse of that trend; that is, the higher the static axle load, generally the lower the impact force.

| Site | Static Axle Load, tonne | Incremental Impact Force, Once Per Year, kN | Static + Impact Once/year Wheel-rail Force, kN |
|---|---|---|---|
| C1 | 25 | 340 | 465 |
| A1 | 28 | 390 | 525 |
| A2 | 28 | 310 | 445 |
| C2 | 30 | 300 | 445 |
| B | 35 | 210 | 380 |

**Table 1 : Static and Impact Forces, All Sites [6]**

Clearly there are other factors which can significantly affect the forces experienced by a track. It is argued in [5] that Table 1's "reverse" trend is due primarily to the quality of wheel-maintenance practices, the mix of traffic type, and operational practices, at the five sites.

b. The lines in Figure 2 are nearly linear above 100kN incremental impact force, and in fact fit a Weibull function very well as argued in [5, 6].

After fitting Weibull functions to Figure 2, one can extrapolate the curves in the graph to see what the impact forces would be at 0.1, 0.01, 0.001, etc, wheels/annum. The number 0.01 represents 1 wheel per 100 years, so extrapolation to 0.01, for example, enables one to predict what the likely maximum impact force would be on each of the five WID sites if one monitored wheel impacts on those sites for 100 years. This process is very similar to the way engineers forecast a 1-in-100 year wind storm or a 1-in-1000 year earthquake event for design of civil infrastructure, based on data measured over a much shorter time.

c. Examination of the WID data from which Figure 2 was constructed shows that the occurrence of a given magnitude of impact force at a given site was unpredictable. In other words, the forces in the graph were random in their magnitude and rate of occurrence, except that the greater the magnitude of the force, the less likely it occurred, as indicated by the downward slope of the lines in the graph. This inverse relationship between magnitude and frequency of occurrence is found in virtually all natural systems: the bigger an earthquake, or rain event, or hurricane, the less likely it is to occur. Designers of buildings and other civil infrastructure use such relationships to determine the likelihood of a given design event from an assumed frequency of occurrence, known usually as the "return period" of an event.

d. The lines in Figure 2 represent billions of WID measurements, so that the distributions of forces have strong statistical reliability.

Clearly, therefore, it is no more appropriate to assume that the maximum forces experienced by rails can be predicted any more than one can predict the throw of a dice. A more rational approach is for designers to use a probability-based approach which would first find out the risk profile a rail business works to, and would then use that profile to determine an appropriate distribution of wheel-rail forces likely to be experienced by the rail during its lifetime [5, 6].

## 4 PREDICTING FATIGUE STATISTICALLY

Because the distributions in Figure 2 have statistical validity, they can be used as the basis for Monte Carlo simulations [7] for calculating the tension stresses induced in the rails at each site during their lifetimes.

### 4.1. Construction of Simulations

As described earlier, a given wheel-rail impact force can occur at any point in time and at any location along the track.

So, an Excel spreadsheet was constructed with 400,000 rows, with each row representing the passing of one wheel. Five columns were set up representing each of the five sites in Figure 2. A random number between 0 and 1 was generated in one cell in each row, which was multiplied by the total number of wheels per year measured at each site – site A2 had the least at 2.7 million wheels/annum and site B the most at 5.4 million wheels/annum. Figure 2 was then used to convert the result into a corresponding incremental impact force for each simulated wheel passing (ie for each row). To illustrate the process, a portion of the numbers produced in this way is shown in Figure 3. The "Max(kN)" row in Figure 3 shows the maximum impact force from the 400,000 simulations/rows, and each number below that Max(kN) row is the impact force derived from Figure 2 for a given wheel-pass, randomised with respect to time.

| | A1 | A2 | B | C1 | C2 |
|---|---|---|---|---|---|
| No. axles/annum: | 2692308 | 4642857 | 5428571 | 2880000 | 4166667 |
| | Below are all incremental impact forces in kN | | | | |
| Random No. | | | | | |
| **Max (kN)=** | **16** | **39** | **13** | **16** | **15** |
| 0.582409 | 9.40 | 10.19 | 7.74 | 8.07 | 8.30 |
| 0.750741 | 6.65 | 10.99 | 6.97 | 6.95 | 7.36 |
| 0.101399 | 15.51 | 39.34 | 13.01 | 15.81 | 14.79 |
| 0.532871 | 8.17 | 12.87 | 8.01 | 8.47 | 8.63 |
| 0.365625 | 9.84 | 14.94 | 9.14 | 10.14 | 10.03 |
| 0.157260 | 13.57 | 19.56 | 11.69 | 13.87 | 13.16 |
| 0.927565 | 5.72 | 9.83 | 6.33 | 6.01 | 6.57 |
| 0.893032 | 5.88 | 10.04 | 6.45 | 6.18 | 6.72 |

**Figure 3 : Portion of Excel Spreadsheet Simulations of Randomised Impact Forces**

Each impact determined in this manner would not occur at one given point on the rail. A wheel flat can occur at any point around the circumference of a wheel tread, which for typical heavy haul wagons is about 3m to 3.5m in length. In other words, the randomised impact forces shown in Figure 3 could occur at any point within a 3m to 3.5m length of rail centred on the rail cross section at which rail stresses will be calculated.

To simulate the random location of an impact, a second set of 400,000 simulations was constructed. For each of these new 400,000 rows, a random number was generated which was then multiplied by half the circumference of the typical wheels found at each of the five WID sites in Figure 2. Figure 4 illustrates a portion of the spreadsheet of numbers generated. The row titled "Length of track" is equal to the circumference of the wheels running over that site. The first column in Figure 4 lists the random numbers generated between +/-0.5, and the other five columns show the corresponding location of the impact in mm; for example, 370 means that the impact occurred 370mm up track from the reference point at which rail stresses will be calculated; -156 means the impact was located 156mm down track from that reference point on the rail.

| | A1 | A2 | B | C1 | C2 |
|---|---|---|---|---|---|
| Length of track (mm): | 3425 | 3425 | 3050 | 3335 | 3335 |
| Random No | | | | | |
| -0.045578 | -156 | -156 | -139 | -152 | -152 |
| 0.108104 | 370 | 370 | 330 | 361 | 361 |
| -0.199869 | -685 | -685 | -610 | -667 | -667 |
| -0.359931 | -1233 | -1233 | -1098 | -1200 | -1200 |
| -0.319280 | -1094 | -1094 | -974 | -1065 | -1065 |
| -0.134440 | -460 | -460 | -410 | -448 | -448 |
| -0.345975 | -1185 | -1185 | -1055 | -1154 | -1154 |
| 0.363113 | 1244 | 1244 | 1107 | 1211 | 1211 |

**Figure 4 : Portion of Spreadsheet Simulations of Randomised Impact Location**

Each of the two sets of 400,000 rows was therefore able to generate incremental impact forces randomised with respect to time and to location. The random numbers at the left of Figures 3 and 4 were refreshed 10 times, and each time the magnitude and location of the 400,000 forces for each site were captured, giving a total of 4 million impact simulations for each site.

### 4.2. Calculation of Rail Foot Tension Stresses

After obtaining the simulated incremental impact force data as described above, each incremental impact force was then added to the relevant static wheel force to produce the total wheel-rail force experienced by the rails at each of the five sites for each impact event. The next step was to use those total forces to calculate the tensile bending stresses in the foot of the rails for each of the 4 million simulations at each site.

To determine rail bending stresses for a given impact force event, the best method is a full dynamic finite element analysis of the track, but that is impossible in this case because there are millions of simulated impact events. Instead, a beam on elastic foundation (BOEF) approach was used because it is simple to use in Excel and is well-accepted by track engineers.

The well-known BOEF formulas for determining rail bending moments are shown in Equations 1 and 2 [8].

$$M = (P.e^{-\beta x}/4\beta).(\cos\beta x - \sin\beta x) \quad (1)$$

$$\beta = (k/4.E.I)^{0.25} \quad (2)$$

where M is the rail bending moment, P is the magnitude of the wheel-rail force, x is the distance to the force from the rail section where stresses are to be calculated, k is the track modulus, E and I are respectively the elastic modulus and moment of inertia of the rail. A sample of the rail stresses calculated from the randomised wheel-rail forces from section 4.1 above, is shown in Figure 5, which also includes some information about the characteristics of each site.

In Figure 5, the track modulus has been nominated for each site as 45MPa, because all tracks were high quality and well maintained, with concrete sleepers, around 250mm of hard rock ballast, capping layer, and improved formation.

| | A1 | A2 | B | C1 | C2 |
|---|---|---|---|---|---|
| Rail size (kg/m): | 60 | 60 | 68 | 60 | 60 |
| Tonnes/axle: | 26 | 28 | 35 | 25 | 30 |
| MGT/annum: | 70 | 130 | 190 | 72 | 125 |
| Sleeper spacing (mm): | 685 | 685 | 610 | 667 | 667 |
| Track modulus (MPa): | 45 | 45 | 45 | 45 | 45 |
| Length of track (mm): | 3425 | 3425 | 3050 | 3335 | 3335 |
| Random No | Below are all max total bend stress rail foot MPa | | | | |
| Static foot stress: | 73.7 | 79.4 | 85.2 | 70.9 | 85.0 |
| **Max (MPa)=** | **201** | **251** | **146** | **199** | **190** |
| -0.045578 | 52.9 | 56.9 | 64.2 | 51.0 | 60.7 |
| 0.108104 | 24.5 | 27.1 | 36.3 | 24.7 | 29.5 |
| -0.199869 | -0.8 | -1.0 | 8.2 | 0.3 | 0.3 |
| -0.359931 | -16.0 | -17.7 | -15.2 | -15.3 | -18.1 |
| -0.319280 | -14.8 | -16.4 | -11.9 | -13.9 | -16.4 |
| -0.134440 | 16.4 | 18.3 | 27.5 | 17.0 | 20.0 |
| -0.345975 | -15.4 | -17.0 | -14.0 | -14.6 | -17.4 |
| 0.363113 | -15.8 | -17.4 | -15.2 | -15.1 | -18.0 |

**Figure 5 : Portion of Spreadsheet of Rail Bending Stresses from Random Forces**

Positive stresses in Figure 5 are tension, but there are also many negative (compression stress) values; when an impact force is located more than 2 or 3 sleepers away, the section of the rail where stresses are being calculated is forced into negative bending, causing the foot of the rail to be in compression. Note also that the stresses in Figure 5 are only for bending of the rail about its major axis; that is, due solely to the application vertical load. Also, for simplicity, variations in track bed support have not been included.

The row titled “Max (MPa)” in Figure 5 lists the maximum bending stress in the foot of the rail from that set of 400,000 simulations, due solely to the incremental impact forces. The row titled “Static foot stress” lists the tensile bending stress in the foot due solely to the static weight of the passing train. When comparing the maximum impact stress with the static stress for each site, there is no obvious relationship between the two. For example, site B has the largest static stress but the lowest maximum impact stress. Sites A2 and C2 are almost identical in track and traffic so their static stresses differ by only 8%, but their maximum impact stresses differ by 35%. As discussed earlier, it is clear that the forces on the rails are not simply a function of the static weight of the train, but are affected in a significant way by other factors such as operational issues.

Figure 5 shows the tensile stresses generated in the rail foot due to vertical bending, but within rails in track there are other tensile stresses which add to these vertical bending stresses.

Firstly, there are residual tensile stresses from rail manufacture, on-site heat treatments, bending of the rails to fit curves, welding, etc. Esveld [9] described how residual stresses can be of the order of 100 to 300MPa in new rail, but also that they can change significantly under the passage of traffic over time. Esveld also stated that the European rail standard limits residual stress to 250MPa in the centre of the rail foot.

Marich [3] suggested that testing of the strength of full-scale samples of rail should account for any effects of residual stresses present in the rail and therefore such stresses may not need to be considered. In practice, it is not uncommon to use perhaps 60MPa as an allowance for residual tension stresses.

Tensile stresses in the rail are also generated in CWR track when the temperature of the rail is at its lowest. The rail temperature can easily swing from its highest to lowest by as much as 70°C, so it is normal to set the rail's stress free temperature (SFT) at a point about half way between the two extremes. A drop of 35° below the SFT is not uncommon, and it will lead to tensile stresses of around 80MPa in the rail cross section.

All of this assumes, of course, that the track is well-maintained and that the SFT is checked regularly and kept at the specified value either by testing or by monitoring of rail longitudinal creep. Kish [10] has shown, however, that it is very difficult to maintain tight control over the SFT.

Another source of tensile stress in the rail foot is from the lateral forces applied by a train's wheels to the head of the rail, causing sideways bending of the rail. These lateral forces arise from dynamic actions of the bogie and train in straight track and from centrifugal actions around curves. Because the edge of the rail foot is the furthest point away from the central vertical axis of the rail, then tensile stresses due to lateral bending are greatest in the edge of the foot. It is common to assume that lateral forces in straight track are around 10% of the normal vertical forces applied by the wheel [3]. But because lateral rail bending is heavily affected by the stiffness of the rail-sleeper fastenings and little is known about the fastenings at the five sites, this effect is not considered in this paper.

A final significant source of tensile stress arises from the location of the wheel on the rail. Good track design and maintenance aims to keep the contact patch between the wheel and rail sitting over the central axis of the rail, but wear of the wheels and rail often results in the contact patch moving away from that axis. The consequence is torsional moments in the rail which generate additional tensile stresses in the rail foot. This effect will also not be considered in this paper due little being known about the factors affecting the magnitude of torsional moments in the rails at the five sites.

### 4.3. Predicting Fatigue Failure

#### 4.3.1. Fatigue damage criterion

Miner's rule is a well-known, straightforward and widely used model for assessing cumulative damage from fatigue [11]. In its simplest form it can be expressed as Equation 3.

$$W_{failure} = N_i \times S_i \quad (3)$$

where $W_{failure}$ is a measure of the total accumulated damage, and $N_i$ is the number of cycles to failure at stress $S_i$. Equation 3 can be applied to fatigue data from rail steel to determine an overall $W_{failure}$. However, Equation 3 does have its drawbacks, as shown when it is applied to the data points in Figure 1: the simple product of stress x cycles to each data point results in widely varying values of $W_{failure}$. Instead, a small modification of Miner's rule provides a more reasonable application to the data in Figure 1. That modification is shown in Equation 4.

$$W_{failure} = \log(N_i) \times S_i \quad (4)$$

Applying Equation 4 to the data in Figure 1, and extending it to apply to 900MPa grade steel which is more typical for heavy haul lines, gives values for $W_{failure}$ which vary only from 3100 to 3500, with a mean $W_{failure}$ of 3350. This value of $W_{failure}$ will be used as the criterion for determining potential fatigue failure in the rails at the five sites being examined in this paper.

#### 4.3.2. Fatigue stress limit

Although Figure 1 illustrates that there is no clear endurance limit for rail steels, it was shown earlier that $10^8$ cycles of load on heavy haul lines is perhaps the maximum that can be expected during the life of a rail these days. Allowing for the scatter of results in Figure 1, about 300MPa could be considered the fatigue limit for $10^8$ cycles. Various studies [3, 4] suggest that the fatigue limit can be determined from Equation 5.

$$\text{Fatigue limit} = 0.4 \times \text{UTS} \quad (5)$$

For 700MPa steel, Equation 5 calculates that the fatigue limit is 280MPa, which is close to the value of 300MPa derived from Figure 1; the limit for 900MPa rail steel is 360MPa. So, to simplify the study of fatigue in the rails at the five sites being examined here, Equation 5 will be used to provide a limit of stress, which if stresses stay below that limit, fatigue failure will be assumed not to occur.

However, 360MPa cannot be considered the limit of bending stress in a rail, below which fatigue failure will not occur. It was shown earlier that residual stresses and temperature induced stresses should also be included. Values of 60MPa for potential residual stresses in the rail and 80MPa for temperature were nominated. Consequently, a suitable bending stress for the sake of this study, below which fatigue failure is assumed not to occur, is 360-60-80=220MPa.

#### 4.3.3. Fatigue prediction for the five sites

In Figure 5 earlier it was shown how bending stresses were determined in the rails at the five study sites, randomised in time and location according to the actual measured wheel-rail force distributions in Figure 2. These stresses can be plotted against the number of wheel passes for each site; the result is shown in Figure 6.

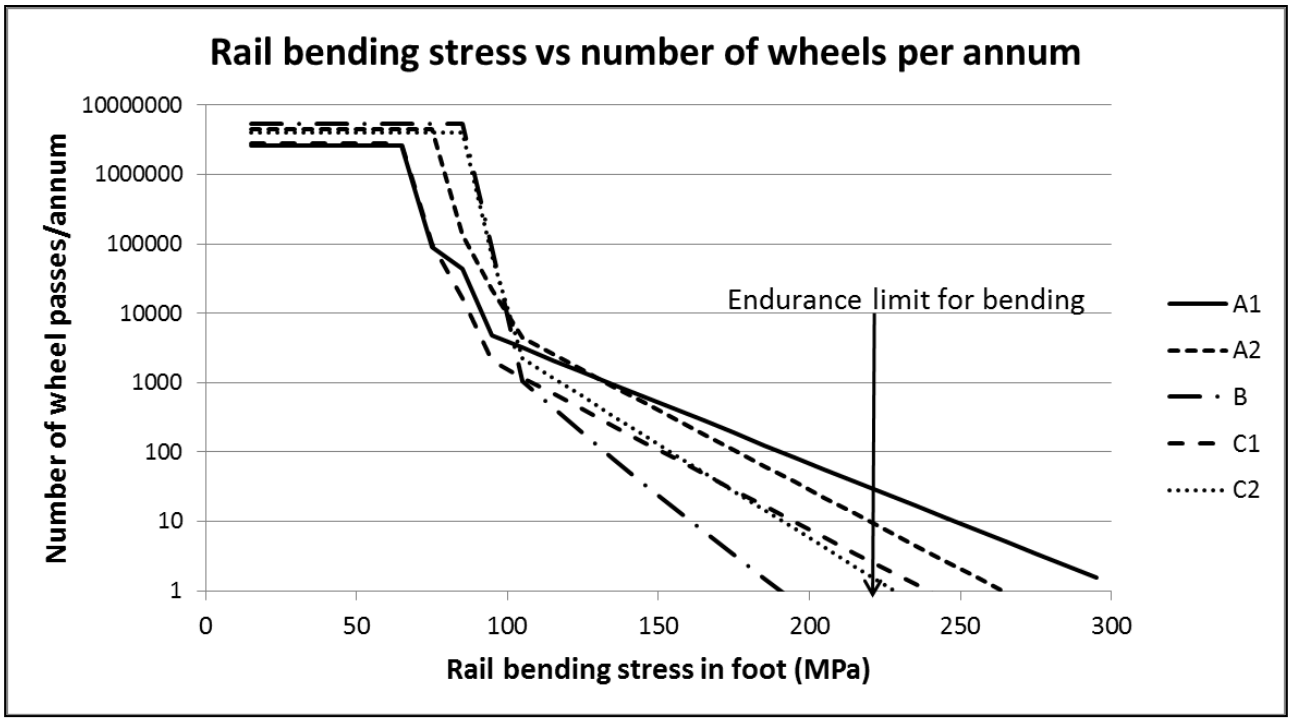


**Figure 6 : Rail Foot Maximum Bending Tension Stress vs Number of Wheel Passes/Annum**

At all five sites, the track designers/maintainers would have chosen the size and type of rail with the intention that fatigue failure would not occur during the life of the rails. However, for the 220MPa bending stress fatigue limit derived in section 4.3.2, it can be seen from Figure 5 that all but one of the sites was exceeding that limit between 2 and 30 times per year. In other words, at sites A1, A2, C1 and C2 fatigue damage was accumulating every year from high stress cycles from very large impact forces. Interestingly, site B was the only one not exceeding the endurance limit and yet it was the site which carried the greatest axle loads and traffic volumes.

In Figure 6, each bending stress value above 220MPa was multiplied by the log of the number of cycles per annum corresponding to that stress. The sum of the resulting values, $\Sigma(\log(N_i) \times S_i)$, is a measure of the fatigue damage accumulated in the rail over the space of one year. This damage would then continue to accumulate year by year, as shown in Figure 7. The fatigue damage limit of 3350, established in section 4.3.1 from application of Miner's rule, is also shown on the graph.

Figure 7 shows site B accumulating no damage, because its maximum bending stress in the rail foot did not exceed 220MPa at any time. The graphs shows sites C1 and C2 gathering increasing fatigue damage but not at a rate to cause damage in the first decade or two of life.

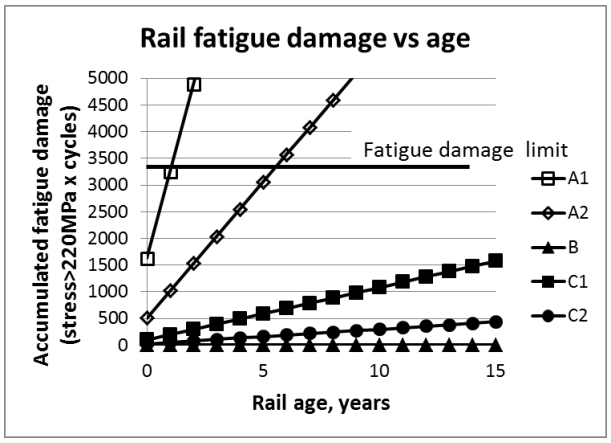


**Figure 7 : Accumulation of Fatigue Damage.**

Sites A1 and A2 are both shown as reaching the fatigue damage limit: A1 at an age of 3 years and A2 at an age of 7 years.

The implications arising from Figures 6 and 7 are discussed in section 5 below, but before doing so the discussion must be tempered with consideration of other factors not included above:

- The bending stresses calculated in the rail from the BOEF method are always higher than those from a full dynamic analysis of very short high impact wheel-rail forces, such as experienced from wheel flats. The mass of the wheel and the mass of the rail cause inertial effects which reduce the actual maximum bending moment, and bending stresses, in the rail.

- Also from a perspective of dynamic behaviour under impact, the BOEF method does not allow for the significant bending moments generated along the rail as the rail vibrates under those impacts. The number of cycles of stress at any cross section could therefore be much larger than predicted by the analyses in this paper.
- As noted in section 4.2, these analyses have not included bending stresses at the edge of the rail foot which are caused either by the wheel-rail contact patch being off-centred on the rail head, or by lateral bending of the rail under sideways forces. Such stresses would increase the accumulated damage in the rail foot.

## 5 FATIGUE, AND OPERATIONAL FACTORS

In Figure 5 the characteristics of each site were presented, and they are shown in Figure 8 for ease of reference in the discussion following.

| | A1 | A2 | B | C1 | C2 |
|---|---|---|---|---|---|
| Rail size (kg/m): | 60 | 60 | 68 | 60 | 60 |
| Tonnes/axle: | 26 | 28 | 35 | 25 | 30 |
| MGT/annum: | 70 | 130 | 190 | 72 | 125 |
| Sleeper spacing (mm): | 685 | 685 | 610 | 667 | 667 |
| Track modulus (MPa): | 45 | 45 | 45 | 45 | 45 |
| Length of track (mm): | 3425 | 3425 | 3050 | 3335 | 3335 |

**Figure 8 : Characteristics of Each Site**

Comparison of sites A1 and C1 shows that they were almost identical in every aspect of track and of traffic loading. As well, sites A2 and C2 show almost identical characteristics. It is not shown in Figure 8, but all five sites had trains operating at 70 to 80km/h, and all had regular, good quality programs of track maintenance. Consequently, according to the normal method of designing against fatigue described in section 3.1, sites A1 and C1 would be expected to demonstrate the same degree of fatigue cracking in the rail foot, or lack thereof, as indeed would sites A2 and C2.

However, Figure 6 showed significant differences in the maximum bending stress in the rail foot for these two sets of nominally identical sites. For the first set, A1's maximum bending stress experienced during one year's traffic was 300MPa whereas C1's was only 240MPa; also, A2's maximum over one year was 260MPa but C1's was only 225MPa.

Multiplying the stresses and cycles of Figure 6 using Miner's rule, as described in section 4.3.1, produced Figure 7 where the differences within the two sets of nominally identical sites was shown very clearly. Site A1 exceeded the fatigue damage limit after 3 years, but its twin C1 would not have exceeded that limit until about 33 years of life. The difference is even more significant for sites A2 and C1, in that A2 exceeded the damage limit after only 7 years but site C1 would not have done so until about 110 years of life.

These analyses are drawn from the real-time measurements of actual on-track wheel-rail forces shown in Figure 1, so the differences in the fatigue behaviour in these two sets of nominally identical sites are very real. The normal method of rail selection does not include parameters or processes which can account for these differences.

In section 3.3 earlier, it was described how the differences between the wheel-rail forces measured at the five sites were due more to operational factors than anything else. The following points demonstrate why this conclusion can be drawn.

- Sites A1, A2. These sites are on different heavy haul lines owned by the same company and operated nominally according to the same standards. However, site A1 had unit mineral trains comprising 22TAL and 28TAL wagons, as well as a mix of passenger and freight trains, which was a much more difficult set of wheels to maintain to a given standard than the A2 site which carried almost exclusively unit mineral trains of 28TAL wagons. This is illustrated by the impact forces at site A1 in Figure 1 being notably greater than at site A2.
- Sites C1, C2. These were actually the one WID site but are sets of data taken 4 years apart; traffic on the line was operated by companies that were independent of the track owner. Between 2007 (C1) and 2011 (C2) the owner and operators worked together to achieve a 70% increase in the annual tonnage on this line and a 20% increase in maximum axle load. These increases coincided with ongoing changes in operating policy, which are reflected in Figure 1 by the lack of increase in the maximum wheel-rail force, and in the corresponding maximum bending stress in Figure 6, despite greater axle loads and traffic. These improvements are illustrated in Figure 7 in that C2 has a much lower rate of accumulation of fatigue damage than C1.
- Site B. This 35TAL line was privately owned by the operator and the traffic was entirely unit mineral trains. The operator had full control over standards, policies and maintenance practices regarding wheel defects, as well as control over driver training and supervision. This high level of control is reflected in the much lower impact forces for this site in Figure 1 and in the lack of fatigue damage in Figure 7, due most likely to the much less severe range of wheel defects in the company's wagon fleet.

Operational practices therefore can have a very strong influence over the magnitude and frequency of impact forces on track and, consequently, over the fatigue life of the rails.

On a final note, rails on heavy haul lines do not have unlimited life and so the growth of fatigue damage, no matter how great or small, cannot continue indefinitely. Assuming that the upper limit of rail life could be as high as 1500MGT, as discussed in section 3.2, one can predict the maximum life of the rails due to the traffic in MGT/a on each site, as listed in Figure 8. The results are shown in Table 2, together with the anticipated fatigue life of the rails determined earlier.

| Site | Age (years) to fatigue limit | Age (years) to 1500MGT |
|---|---|---|
| A1 | 3 | 21 |
| A2 | 7 | 12 |
| B | ∞ | 8 |
| C1 | 33 | 21 |
| C2 | 110 | 12 |

**Table 2 : Fatigue Age vs Wear Age.**

Despite accumulating fatigue damage, the rails at sites B, C1 and C2 would need to be replaced due to loss of head section area long before fatigue became a problem. But for sites A1 and A2, rail breaks due to fatigue would be likely to occur before the rails wore out; at site A1 fatigue cracking would likely be of great concern. Unfortunately, maintenance data at all five sites is treated highly confidentially, so that it has not been possible to obtain confirmation of these deductions from the owners or operators.

## 6 CONCLUSIONS

Fatigue of the steel in the foot of a rail is dependent upon the magnitude of the tension stresses in the foot, and the number of cycles of stresses induced in the foot. Traditional rail selection procedures assume that the maximum stress in the foot is entirely predictable, but the paper shows that this is not so.

Data from billions of measurements of actual wheel-rail impact forces from a number of heavy haul sites has shown that those forces are randomly distributed in magnitude, time and location, and thus the bending stresses they induce are likewise randomly distributed. Furthermore the magnitude of these stresses has been found to be dependent not only on axle loads and track characteristics, but also on operational factors such as the mix of traffic, wheel maintenance policies and practices, and perhaps even driver behaviour.

Traditional rail selection ignores these operational factors which is one reason why the appearance of rail fatigue has been so hard to predict.

Large scale Monte Carlo simulations of tension stresses in the rail foot have been undertaken based on that statistically significant wheel-rail impact data. The simulations have identified the effect of operational factors on the likelihood of fatigue failure in the rails at the five sites. Importantly, sites which would be deemed almost identical using traditional rail stress analyses are found to be likely to have dramatically different fatigue histories.

## 7 REFERENCES

1. Kazymyrovych V. Very high cycle fatigue of engineering materials. Karlstad University Studies, Sweden. 2009:22.
2. Campbell FC (ed). Elements of metallurgy and engineering alloys. ASM International, Ohio. 2008.
3. Marich S. Rail and related track structures. Study Notes. Queensland University of Technology, Brisbane. 2007.
4. Dang Van K., Cailletaud G., Flavenot J.F., Le Douaron A., Lieurade H.P. Criterion for high cycle fatigue failure under multiaxial loading. Biaxial and Multiaxial Fatigue. EGF 3, Mechanical Eng. Publications, London, 1989.
5. Murray M. Managing the track asset through wheel maintenance. Proceedings of the Conference on Railway Engineering, Railway Technical Society of Australasia. Brisbane, Australia: Sept 2012.
6. Murray M. Rational sleeper design method for heavy haul. IHHA 2015 Conference, Perth, 21-24 June. International Heavy Haul Association. 2015.
7. Landau D.P, Binder K. A guide to Monte Carlo simulations in statistical physics. Cambridge University Press. Cambridge UK. 2000.
8. Doyle N.F. Railway track design; a review of current practice. Bureau of Transport Economics, Occasional Paper 35. Commonwealth of Australia. Canberra. 1980.

9 Esveld C. Modern railway track. 2nd ed. MRT Productions. Netherlands. 2001.

10 Kish A., Samavedam G. Risk analysis based CWR track buckling safety evaluations. Proceedings of International Conference on Innovations in the Design & Assessment of Railway Track, December 2-3. Delft University of Technology. Netherlands. 1999.

11. Miner MA. Cumulative damage in fatigue, Journal of Applied Mechanics, Vol. 12, American Society of Mechanical Engineers, New York: 1945.